Fault zone structure of the central Alpine Fault revealed during the first phase of the Deep Fault Drilling Project (DFDP-1)

John Townend[1], Rupert Sutherland[2], Virginia G. Toy[3], Simon C. Cox[4], Carolyn Boulton[5], Jennifer D. Eccles[6], David McNamara[7]

[1]School of Geography, Environment, and Earth Sciences, Victoria University of Wellington (john.townend@vuw.ac.nz), [2]GNS Science, Lower Hutt, [3]Department of Geology, University of Otago, Dunedin, [4]GNS Science, Dunedin, [5]Department of Geological Sciences, University of Canterbury, [6]Institute of Earth Sciences and Engineering, University of Auckland, [7]GNS Science, Wairakei

ECGS Workshop 2012, Luxembourg

1 Introduction: background and motivation

Understanding what conditions prevail within the interiors of active faults is crucial for elucidating the mechanisms governing long-term fault evolution and, in particular, the earthquake-rupture processes that are of vital interest to society.

The Alpine Fault (Figure 1) is a mature, transpressive plate-bounding structure that has accommodated >460 km of dextral offset since 24 Ma and which has a late Quaternary slip rate of c. 26 mm/yr[1]. Paleoseismic observations indicate that the Alpine Fault produces large earthquakes ($\mathbf{M}_W$~8) every 200–400 years and that it last slipped in 1717 AD[2,3].

The Deep Fault Drilling Project (DFDP) is focused on determining the conditions under which faults evolve and generate earthquakes, via a sequence of drilling operations and long-term monitoring permitting analysis of ambient conditions and fault rock lithologies near the central Alpine Fault[4].

In contrast to several fault zone drilling experiments undertaken following large earthquakes, DFDP addresses conditions in an active fault zone *prior to* an anticipated large earthquake.

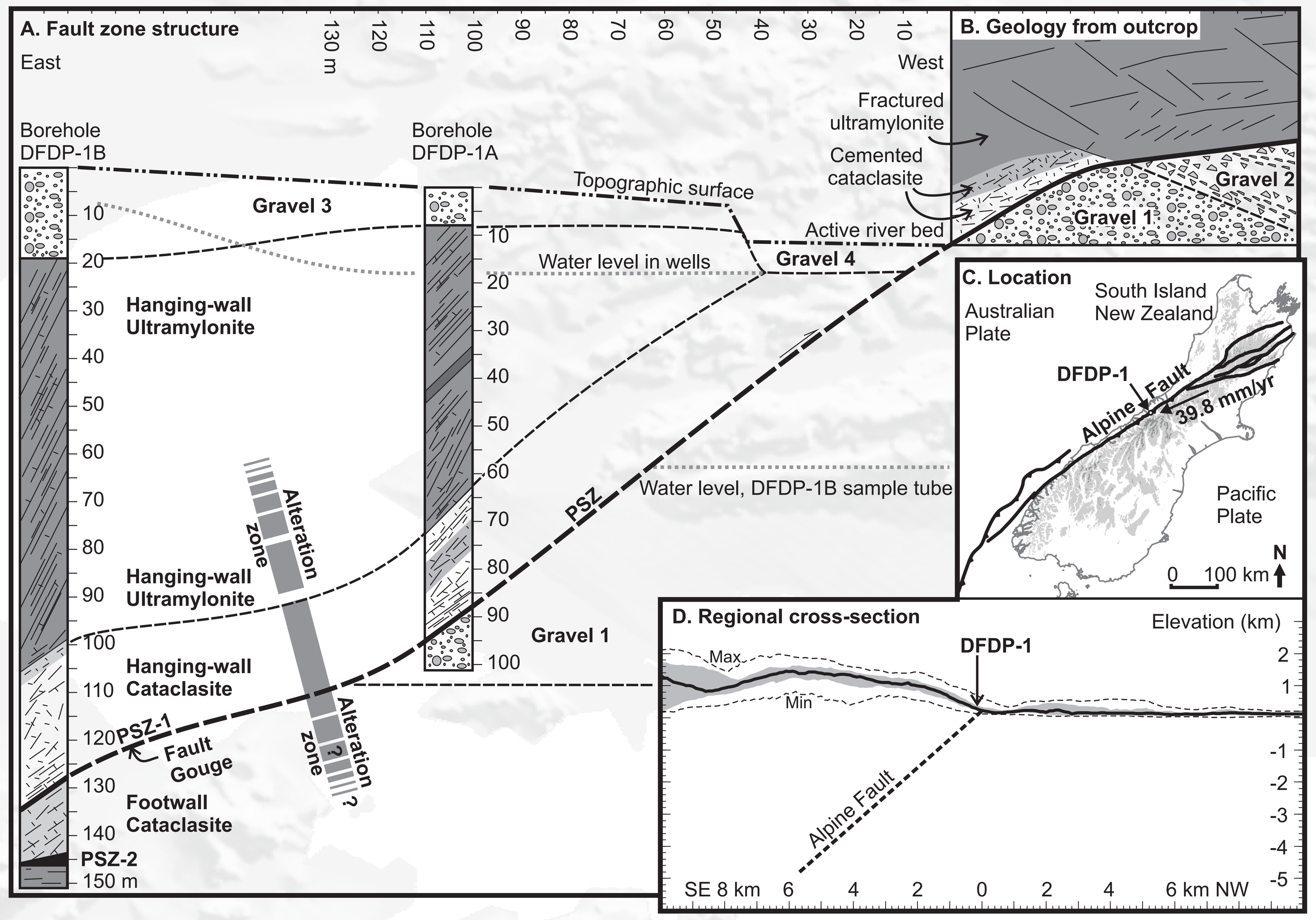

Figure 1 Integrated cross-section through DFDP-1 boreholes (A) and outcrop geology (B). The bold line marks the principal slip zone (PSZ) intersected in both boreholes. Map (C) shows the location of the DFDP-1 experiment. Inset (D) shows median topography within 10 km of DFDP-1 (central 50% shaded) projected normal to the Alpine Fault.

2 Observations from DFDP-1

The first phase of DFDP drilling (DFDP-1) was completed in February 2011 with the construction and instrumentation of two shallow boreholes intersecting the central Alpine Fault at Gaunt Creek[5].

Core analysis and wireline logging data (Figure 2) reveal the presence of a mineralogically and hydrologically distinct 15–20 m-thick "alteration zone" in the hanging wall formed by fluid-rock interaction and mineralization. This alteration zone is formed of cemented low-permeability fractured ultramylonite and cataclasite, and obscures the boundary between the damage zone and fault core. The fault core contains a <0.5 m-thick principal slip zone (PSZ) at a depth of 128 m, near the base of a 2 m-thick layer of gouge and ultracataclasite.

The gouge exhibits markedly different properties from the rocks above and below, particularly with respect to density (lower by c. 0.3 g/cc than in the other cored lithologies), neutron porosity (a factor of almost two higher) and, most distinctively, low electrical resistivity, high spontaneous potential, and low seismic velocity (by c. 1 km/s). The single footwall lithology cored in DFDP-1B exhibits the lowest mean seismic velocity and density of all lithologies other than the gouge.

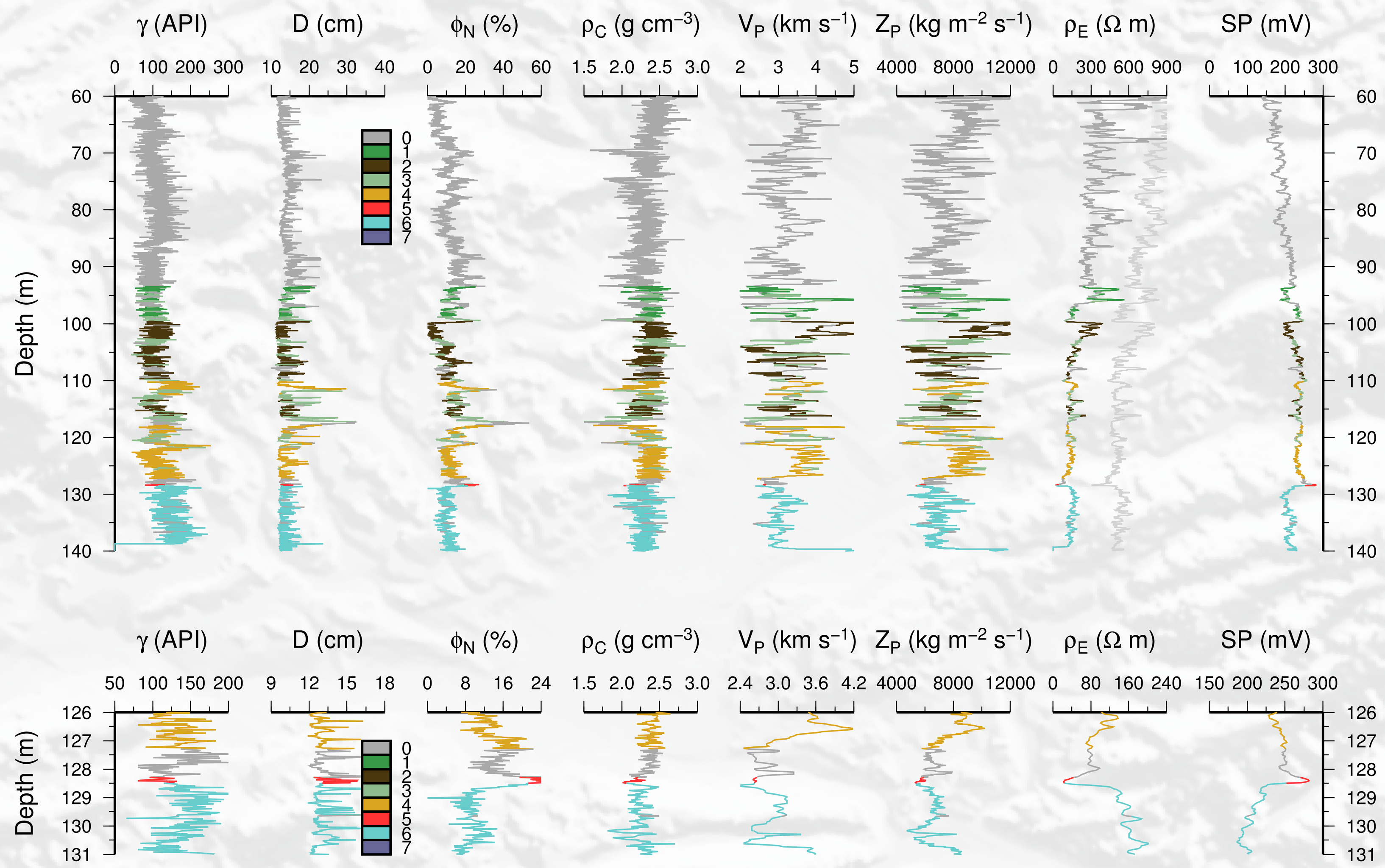

Figure 2 (Top) Depth profiles of wireline logging parameters in DFDP-1B, colored according to the lithology determined from core analysis. From left to right, the curves show natural gamma (γ), borehole diameter (D), neutron porosity (Φ_N), compensated density (ρ_C), P-wave velocity (V_P), P-wave impedance ($Z_P = V_P\rho_C$), electrical resistivity (ρ_E), and spontaneous potential (SP). (Bottom) A zoomed view of the 128 m PSZ, which was also intersected in DFDP-1A

The geometry and distribution of fractures identified in DFDP-1B are illustrated in Figure 3. Overall, most fractures dip E- or SE-ward, consistent with the gross fault orientation inferred from surface outcrops and the borehole intersection depths. Core recovery in the 50–100 m interval was poor, and the borehole became significantly enlarged (cf. Figure 2), so the high fracture density above 100 m may reflect a combination of lithologic and drilling-related factors. Below 100 m, the inferred fracture decreases systematically towards the PSZ and into the footwall below.

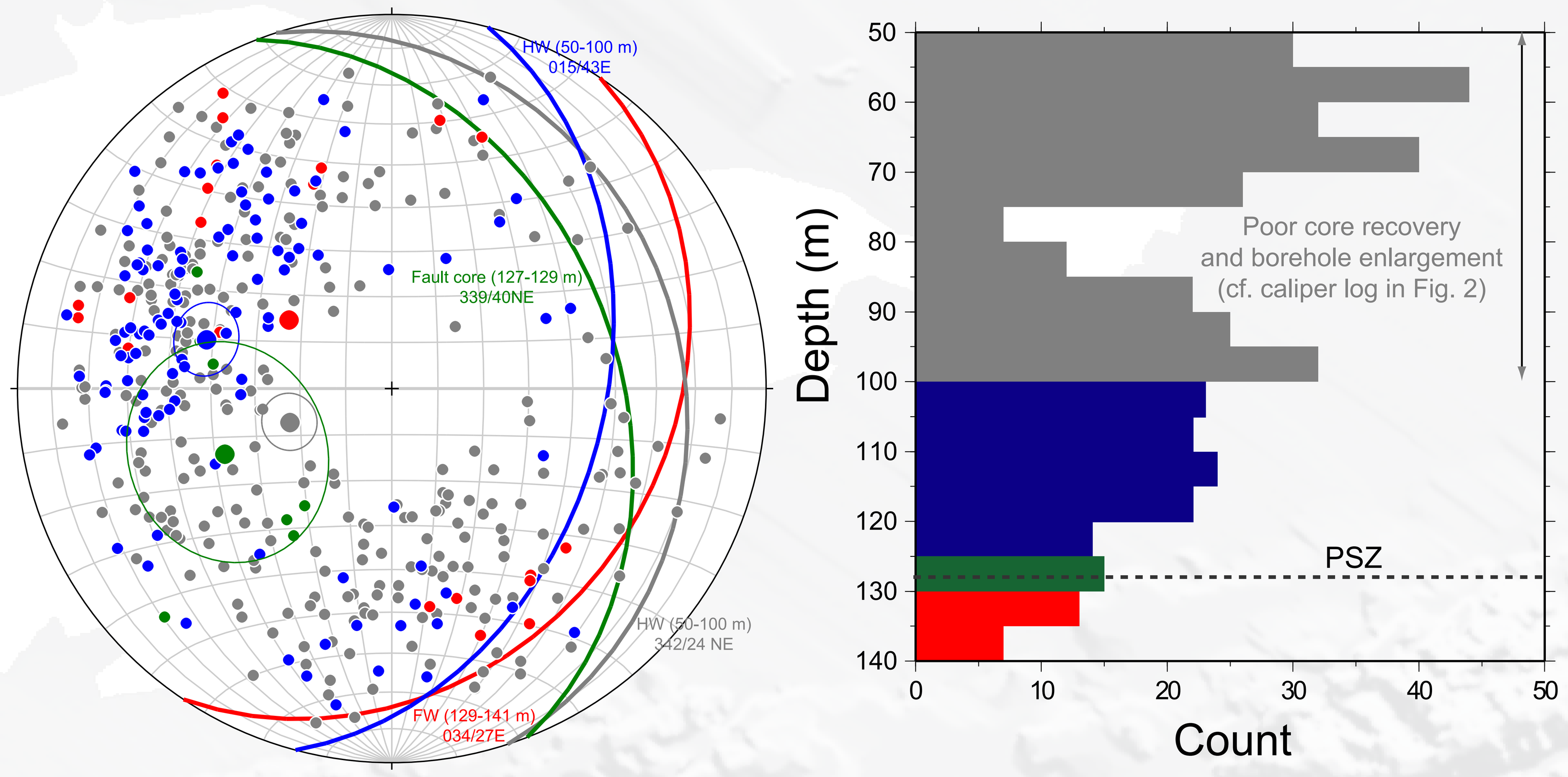

Figure 3 (Left) Summary of fracture orientations in DFDP-1B determined from analysis of borehole televiewer images. The pole to each fracture is plotted as a dot colored according to depth: 50–100 m — gray; 100–127 m — blue; 127–129 m — green; 129–141 m — red. 'HW' and 'FW' denote the hanging wall and footwall, respectively. The large symbols illustrate the mean poles and 95% confidence circles, and the great circles show the corresponding mean fracture planes. (Right) Fracture density as a function of depth in DFDP-1B, colored as in the left-hand image.

Hydraulic observations made during drilling, piezometer measurements made over 12 months as fluid pressures equilibrated, and laboratory data all yield consistent estimates of the fault core's permeability of c. 10^{-23} to 10^{-21} m^2. In contrast, the permeability determined via slug tests in the distal damage zone 50 m above the PSZ is c. 10^{-14} m^2; in other words, a six order-of-magnitude permeability difference exists across the alteration zone. The decrease in permeability across the alteration zone appears to be governed by a downward increase in phyllosilicate and carbonate materials in fractures. A pressure difference of c. 0.5 MPa exists across the PSZ (Figure 4), indicating that it currently forms an impermeable seal within the low-permeability alteration zone.

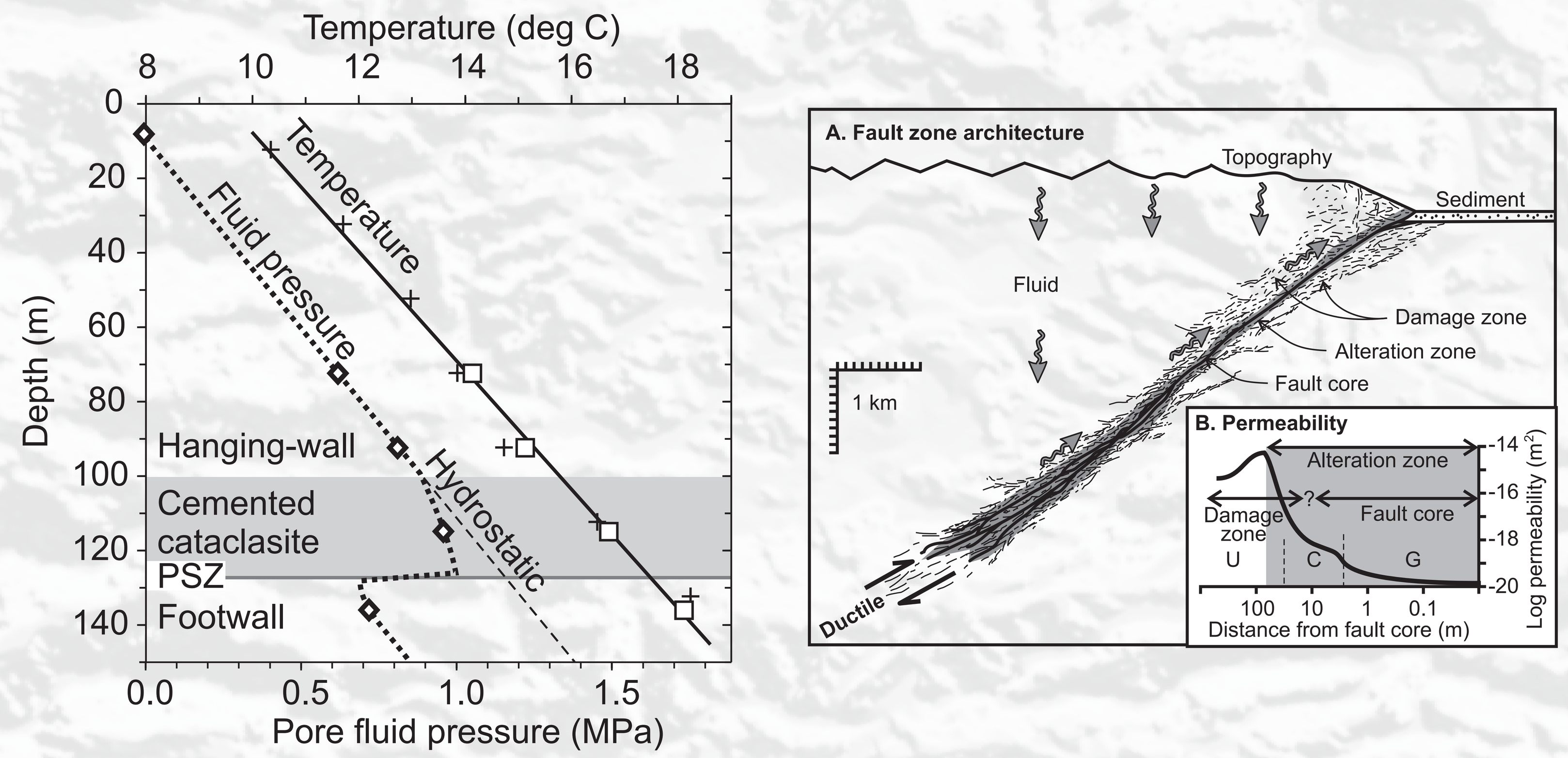

Figure 4 (Left) Fluid pressures (diamonds) in DFDP-1B and temperatures (crosses and squares, representing different sensor types) after one year of equilibration. (Right) Schematic drawing of an oblique reverse fault based on DFDP-1 observations showing the damage zone, alteration zone (shaded), and fault core. Permeability is low in the alteration zone (B, inset). Dashed lines (inset) show lithologic boundaries: hanging-wall ultramylonite (U); cataclasite (C); gouge and ultracataclasite (G).

3 Discussion

The extremely low permeability and meter-scale width of the fault core are likely to play a significant role in governing earthquake rupture on the central Alpine Fault. In particular, the permeability of $<10^{-21}$ m^2 we infer for the 2 m-thick fault core enclosing the PSZ suggests that the fault may undergo extreme thermal pressurization behavior in response to small amounts (possibly submillimeter) of slip at low slip rates ($\ll$1 mm/s) well before the onset of seismic radiation[6,7].

The wireline and fracture data illustrated in Figures 2 and 3 reveal macroscopic (1–100 m-scale) asymmetry and indicate that the footwall within c. 10 m of the PSZ is more compliant (less stiff) than the hanging wall at comparable distances from the principal slip zone. The coincidence of higher seismic velocities and greater fracture density in the hanging wall is consistent with some models of cumulative deformation on asymmetric fault zones[8,9]. Moreover, the asymmetry may affect rupture and seismic wave propagation within the fault zone, coseismic changes in fault strength and ground motion distributions[10–13].

Further characterizing the structural and hydraulic architecture of the fault zone will improve our understanding of the relationship between in situ conditions, earthquake rupture processes, and the hazards posed by future Alpine Fault earthquakes.

References

1. Sutherland, R., Berryman, K., and Norris, R. *Geological Society of America Bulletin* **118**(3–4), 464–474 (2006).
2. Sutherland, R., Eberhart-Phillips, D., Harris, R., et al. In *A Continental Plate Boundary: Tectonics at South Island, New Zealand*, Okaya, D., Stern, T., and Davey, F., editors, number 175 in Geophysical Monograph Series, 235–251. American Geophysical Union (2007).
3. Berryman, K., Cochran, U., Clark, K., Biasi, G., Langridge, R., and Villamor, P. *Science* **336**(6089), 1690–1693 (2012).
4. Townend, J., Sutherland, R., and Toy, V. *Scientific Drilling* **8**, 75–82 (2009).
5. Sutherland, R., Toy, V., Townend, J., et al. *Geology* (2012). 10.1130/G33614.1.
6. Segall, P. and Rice, J. R. *Journal of Geophysical Research B: Solid Earth* **111**(9) (2006).
7. Schmitt, S., Segall, P., and Matsuzawa, T. *Journal of Geophysical Research B: Solid Earth* **116**(6) (2011).
8. Dor, O., Yildirim, C., Rockwell, T., Ben-Zion, Y., Emre, O., Sisk, M., and Duman, T. *Geophysical Journal International* **173**(2), 483–504 (2008).
9. Mitchell, T., Ben-Zion, Y., and Shimamoto, T. *Earth and Planetary Science Letters* **308**(3-4), 284–297 (2011).
10. Ma, S. *Geophysical Research Letters* **36**(20) (2009).
11. Harris, R. A. and Day, S. *Geophysical Research Letters* **32**(23), 1–4 (2005).
12. Ben-Zion, Y. and Shi, Z. *Earth and Planetary Science Letters* **236**(1-2), 486–496 (2005).
13. Ma, S. and Beroza, G. *Bulletin of the Seismological Society of America* **98**(4), 1642–1658 (2008).